
BUSTR: BREAST ULTRASOUND TEXT REPORTING WITH A DESCRIPTOR-AWARE VISION–LANGUAGE MODEL

Rawa Mohammed, Mina Attin, Bryar Shareef
 University of Nevada, Las Vegas

ABSTRACT

Automated radiology report generation (RRG) for breast ultrasound (BUS) is limited by the lack of paired image–report datasets and the risk of hallucinations from large language models. We propose BUSTR, a multitask vision–language framework that generates BUS reports without requiring paired image–report supervision. BUSTR constructs reports from structured descriptors (e.g., BI-RADS, pathology, histology) and radiomics features, learns descriptor-aware visual representations with a multi-head Swin encoder trained using a multitask loss over dataset-specific descriptor sets, and aligns visual and textual tokens via a dual-level objective that combines token-level cross-entropy with a cosine-similarity alignment loss between input and output representations. We evaluate BUSTR on two public BUS datasets, BrEaST and BUS-BRA, which differ in size and available descriptors. Across both datasets, BUSTR consistently improves standard natural language generation metrics and clinical efficacy metrics, particularly for key targets such as BI-RADS category and pathology. Our results show that this descriptor-aware vision model, trained with a combined token-level and alignment loss, improves both automatic report metrics and clinical efficacy without requiring paired image–report data. The source code can be found at <https://github.com/AAR-UNLV/BUSTR>

Keywords Breast Ultrasound · Breast Cancer · Medical Report Generation · BI-RADS · Large Language Models · Zero-Shot Learning · Multimodal · Domain Aware · Radiology Report Generation

1 Introduction

Breast ultrasound (BUS) is a vital complementary imaging tool for early tumor detection, particularly due to its increased sensitivity in dense breast tissue, where mammography tends to be less effective [1]. However, increasing demand for radiological services has created a bottleneck that results in delayed diagnoses, increased workloads, and a higher risk of errors, all of which can negatively impact patient care [2].

Previous BUS computer-aided diagnosis (CAD) systems have mainly focused on lesion segmentation [3, 4] and classification [5], demonstrating the value of curated benchmarks and tumor-aware architectures for downstream analysis [6]. Beyond single-task models, multitask architectures that jointly model tumor classification with auxiliary objectives have shown further gains in representation quality and decision support for BUS [7, 8, 9]. However, these systems mainly produce quantitative outputs (e.g., segmentation masks, class labels or probabilities, and BI-RADS categories) rather than full narrative reports. While such outputs are useful for triage and risk stratification, they provide limited insight into how specific imaging findings support a given decision. In contrast, narrative BUS reports can improve interpretability and clinical explainability by explicitly linking visual descriptors to the final assessment rather than returning only a score or category. To address the growing demand, reporting burden, and need for more interpretable outputs, researchers have therefore explored automated report generation methods to assist radiologists and improve diagnostic efficiency.

Automated radiology report generation (RRG) has evolved from early template-based and retrieval-based approaches [10, 11] to deep learning and transformer-based models [12, 13, 14] and, more recently, large language models (LLMs) [15]. Although template-based and retrieval-based approaches helped standardize reporting, they lacked flexibility beyond predefined patterns. With deep learning [12], early systems paired convolutional neural networks (CNNs) for image feature extraction with recurrent neural networks (RNNs), including long short-term memory (LSTM) networks,

for descriptive text generation. These approaches improved report generation but still struggled to capture long-range dependencies and maintain contextual coherence, and their outputs often remain fragmented and lack the depth needed for clinical interpretation.

Recently, large language models (LLMs) have significantly influenced radiology report generation [16, 15]. They improve text generation, contextual understanding, and multimodal learning, allowing for more coherent reports. Nevertheless, LLM-based systems still struggle with medical image interpretation, sometimes producing incorrect descriptions, irrelevant details, or hallucinated findings [17, 18]. Recent work has begun to address factual consistency by explicitly aligning visual concepts with diagnostic findings [19] or by optimizing report quality and diversity via reinforcement learning and text augmentation [20], but these approaches still rely on large paired image-report corpora. In breast ultrasound, multimodal vision-language approaches have also been explored, for example using text prompts derived from clinical descriptors to guide segmentation [21], which further motivates leveraging structured textual information for BUS report generation.

A major limitation for BUS report generation is the lack of large, well-annotated paired image-report datasets, which makes it difficult to train robust deep learning models. Additionally, manual annotation of BUS images requires significant time and resources, further limiting the availability of such paired data. Although Breast Imaging-Reporting and Data System (BI-RADS) provides a structured, standardized way to describe lesions and supports structured reporting and data mining in clinical practice [22, 23], it does not capture the full diagnostic reasoning process of radiologists. In addition, BUS images are affected by operator dependency, speckle noise, low contrast, and artifacts, which further complicate reliable report generation.

Several studies have explored AI-driven BUS computer-aided diagnosis and report generation [24, 25, 26, 27, 28, 29]. Qin et al. [27] proposed a deep learning-based tumor classification model, but their approach focuses on lesion categorization rather than full-text report generation. Lo and Chen [26] introduced a metadata-driven reporting system that integrates multiple imaging features, yet the resulting outputs remain relatively shallow and lack detailed narrative descriptions. Li et al. [25] developed a cross-modality feature alignment method to enhance text-image coherence, though its reliance on private datasets limits broader applicability. Azhar et al. [28] presented an AI-powered pipeline that synthesizes structured multimodal BUS reports by combining radiologist annotations with deep learning analysis. Huh et al. [29] integrated multiple BUS analysis tools within a LangChain-based LLM framework to generate clinically meaningful breast ultrasound reports. Similarly, Ge et al. [24] incorporated BI-RADS descriptors into structured BUS reporting, but their system mainly produces template-style outputs rather than fully narrative reports.

In this study, we propose BUSTR, a unified multimodal framework for BUS report generation without paired image-report data. The method constructs a fact-grounded vision encoder from structured descriptors with multitask training across heterogeneous datasets, and aligns visual tokens with word embeddings as an instruction prompt into a frozen language model to produce narrative reports. A two-level objective encourages accurate token prediction and sentence-level semantic agreement. Our contributions are as follows:

1. We propose BUSTR, a single framework for BUS report generation without paired image-report supervision.
2. We design a descriptor-aware vision-language alignment module, trained with configuration-specific multitask learning, that supports joint training across multiple BUS datasets with partially overlapping descriptor sets.
3. We introduce dual-level training objective functions that couple token-level cross-entropy with sentence-level semantic agreement, aiming to reduce hallucinations.

2 Proposed Method

2.1 Overview

The proposed framework, BUSTR, consists of three main components: (1) zero-shot report generation, where structured descriptors and radiomics features are converted into BUS reports; (2) multitask BUS descriptor classification, where a vision encoder is trained to predict multiple lesion descriptors and auxiliary targets; and (3) report generation, where vision tokens and prompts are jointly processed to generate clinically meaningful reports using a combination of cross-entropy and cosine-similarity alignment loss. The same framework is applied to both datasets: any structured, textual, or metadata associated with a BUS image is treated as text and used to construct supervisory reports. The overall architecture is shown in Fig. 1.

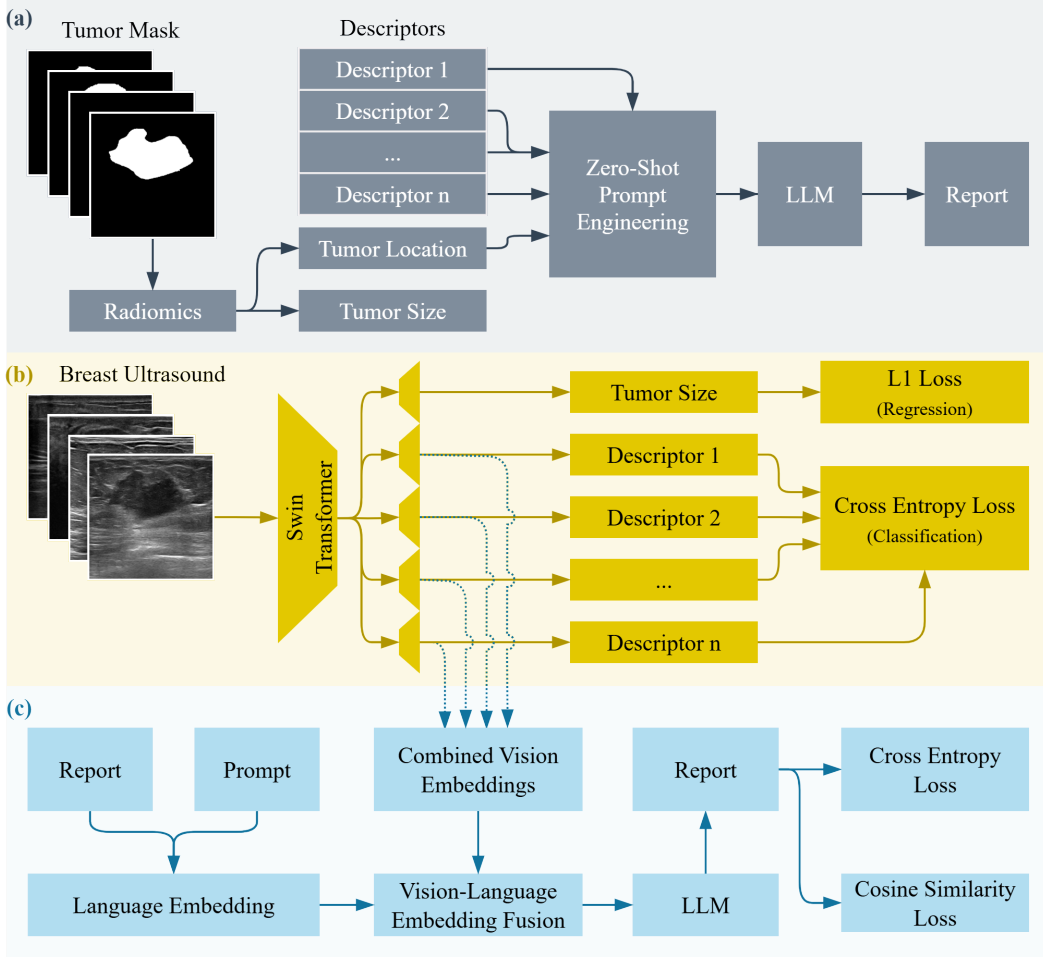


Figure 1: Overall BUSTR architecture. (a) Zero-shot construction of reports from BUS descriptors and radiomics features. (b) Multitask training of a descriptor-aware Swin vision encoder. (c) Report generation, where visual tokens and prompts are fused in a frozen LLM to produce BUS reports.

2.2 Supervisory Report Construction from Structured Descriptors

In the absence of narrative radiology reports for breast ultrasound (BUS) images, we utilize a Llama-based model [30] to generate reports from structured, fact-based BUS descriptors. These descriptors may include BI-RADS information (e.g., BI-RADS class, shape, margin, echogenicity, posterior features), histopathology annotations (e.g., histology and pathology), and radiomics features extracted from tumor masks (e.g., size, intensity statistics). Depending on the image, only a subset of these descriptors may be available. In what follows, we refer to these automatically generated texts simply as *reports*.

The key design principle is that supervisory reports should not introduce any new findings beyond what is present in the structured fields. Unlike generic synthetic reports, our reports are constrained to restate validated descriptor values and radiomics-derived attributes, avoiding unsupported or hallucinated content. Later, we evaluate how well the generated reports preserve these facts using clinical efficacy metrics such as F1-score (F1), precision (P), and sensitivity (S).

For a given BUS image, we collect all available descriptor–value pairs into

$$\hat{y}_{\text{descriptors}} = \{(d, \hat{y}_d)\},$$

where each d denotes a descriptor type (e.g., BI-RADS class, shape, margin, pathology) and \hat{y}_d is its corresponding value. We denote the associated radiomics features by

$$\mathbf{R} = f_{\text{rad}}(M),$$

where M is the tumor mask and $f_{\text{rad}}(\cdot)$ is a fixed radiomics feature extractor.

We define a formatting function $\mathcal{F}_{\text{format}}$ that converts the available descriptors and radiomics features into an instruction-style prompt:

$$P = \mathcal{F}_{\text{format}}(\hat{y}_{\text{descriptors}}, \mathbf{R}), \quad (1)$$

where P is a natural language description of the lesion constructed solely from the structured information for that image. The formatted prompt P is then provided to the frozen LLM to generate the report:

$$R_{\text{gen}} = \mathcal{F}_{\text{LLM}}(P). \quad (2)$$

This construction process is applied identically to all images; the only variation is which descriptor–value pairs (d, \hat{y}_d) appear in $\hat{y}_{\text{descriptors}}$, depending on the dataset and available annotations.

2.3 Multi-head Vision Encoder via Multitask Descriptor Classification

We design a multitask model that uses a pre-trained Swin Transformer [31] as a vision encoder with multiple classification heads and a single regression head. Let $I \in \mathbb{R}^{H \times W}$ be an input ultrasound image, and let

$$\mathbf{E} = f_{\text{enc}}(I) \in \mathbb{R}^{P \times E}$$

denote the encoder output, where P is the number of image patches (vision tokens) and E is the embedding dimension. The Swin encoder is followed by four descriptor-specific branches for shape, margin, posterior features, and echogenicity, as well as a separate branch for tumor size. For each branch, we apply adaptive average pooling over the patch dimension to obtain a fixed-length hidden state (e.g., $\mathbf{h}_{\text{shape}}$, $\mathbf{h}_{\text{margin}}$, $\mathbf{h}_{\text{posterior}}$, \mathbf{h}_{echo}), which is shared across the corresponding prediction heads.

BI-RADS prediction is implemented as a descriptor-aware classifier that takes the concatenation of all four descriptor hidden states:

$$\hat{y}_{\text{BI-RADS}} = h_{\text{BI-RADS}}(\text{concat}(\mathbf{h}_{\text{shape}}, \mathbf{h}_{\text{margin}}, \mathbf{h}_{\text{posterior}}, \mathbf{h}_{\text{echo}})),$$

mirroring the ACR guidelines in which BI-RADS categories are derived from combinations of lesion descriptors. In addition, we define individual classification heads for shape, margin, posterior features, and echogenicity, and a regression head for tumor size:

$$\begin{aligned} \hat{y}_{\text{shape}} &= h_{\text{shape}}(\mathbf{h}_{\text{shape}}), \\ \hat{y}_{\text{margin}} &= h_{\text{margin}}(\mathbf{h}_{\text{margin}}), \\ \hat{y}_{\text{posterior}} &= h_{\text{posterior}}(\mathbf{h}_{\text{posterior}}), \\ \hat{y}_{\text{echo}} &= h_{\text{echo}}(\mathbf{h}_{\text{echo}}), \\ \hat{y}_{\text{size}} &= h_{\text{size}}(\mathbf{h}_{\text{size}}), \end{aligned} \quad (3)$$

where \hat{y}_{size} is a normalized scalar (we scale tumor size by the maximum value during training, consistent with the implementation).

During inference, the tumor size head provides a quantitative size estimate that is inserted into the generated report as a scalar value. Empirically, adding tumor size as an extra vision token for the language model did not improve performance, so it is not included in the visual token sequence.

Multitask Loss

For each supervised target (e.g., BI-RADS category, tumor size, shape, margin, posterior features, echogenicity), we define a separate loss term. Categorical descriptors are optimized with cross-entropy losses, while tumor size is optimized with an L1 loss (mean absolute error) on the normalized size:

$$\begin{aligned} \mathcal{L}_{\text{BI-RADS}} &= \text{CE}(\hat{y}_{\text{BI-RADS}}, y_{\text{BI-RADS}}), \\ \mathcal{L}_{\text{shape}} &= \text{CE}(\hat{y}_{\text{shape}}, y_{\text{shape}}), \\ \mathcal{L}_{\text{margin}} &= \text{CE}(\hat{y}_{\text{margin}}, y_{\text{margin}}), \\ \mathcal{L}_{\text{posterior}} &= \text{CE}(\hat{y}_{\text{posterior}}, y_{\text{posterior}}), \\ \mathcal{L}_{\text{echo}} &= \text{CE}(\hat{y}_{\text{echo}}, y_{\text{echo}}), \\ \mathcal{L}_{\text{size}} &= \text{L1}(\hat{y}_{\text{size}}, y_{\text{size}}). \end{aligned} \quad (4)$$

Some descriptors are composite. In particular, margin includes a main class (circumscribed vs. non-circumscribed) and four non-circumscribed sub-types (indistinct, angular, spiculated, microlobulated). Let $\mathcal{L}_{\text{Margin}}$ denote the loss

for the main margin class, and let $\mathcal{L}_{\text{margin},j}$ denote the loss for subtype j , where $j \in \{1, \dots, 4\}$ indexes the four non-circumscribed sub-types. The combined margin loss is then defined as

$$\mathcal{L}_{\text{Combined Margin}} = 0.5 \mathcal{L}_{\text{Margin}} + \frac{0.5}{4} \sum_{j=1}^4 \mathcal{L}_{\text{margin},j}, \quad (5)$$

which matches the implementation where the main margin loss and the mean of the four subtype losses are averaged with equal weights.

Let $\mathcal{T}^{(\text{cfg})}$ denote the set of supervised tasks used in a given training configuration (e.g., for one dataset, $\mathcal{T}^{(\text{cfg})}$ may include BI-RADS, tumor size, shape, margin, posterior features, and echogenicity; for another dataset, only a subset of these descriptors is available). Let \mathcal{L}_t be the per-task loss, with $\mathcal{L}_{\text{Combined Margin}}$ used for margin. The overall multitask vision loss is defined as the average over the active tasks:

$$\mathcal{L}_{\text{Vision}}^{(\text{cfg})} = \frac{1}{|\mathcal{T}^{(\text{cfg})}|} \sum_{t \in \mathcal{T}^{(\text{cfg})}} \mathcal{L}_t. \quad (6)$$

In the fully annotated configuration, this reduces to the simple average of the six main task losses (tumor size, BI-RADS, shape, combined margin, posterior features, and echogenicity), consistent with the implemented loss.

2.4 Report Generation

The model generates radiology reports, R_{final} , by combining vision embeddings from the pre-trained multi-head vision encoder with word embeddings of the report and an instructional prompt. The word embedding sequence is produced by the LLM’s embedding model \mathbf{E}_{LLM} and defined as

$$\mathbf{E}_{\text{word}} = \mathbf{E}_{\text{LLM}}(T, P),$$

where T is the (partially) generated or ground-truth report text used during training, and P is the instruction-style prompt.

Meanwhile, the vision encoder produces visual tokens \mathbf{E}_v from the ultrasound image, capturing features relevant to the descriptor classification tasks. These visual tokens are projected into LLaMA’s [30] embedding space and concatenated with the word embeddings:

$$R_{\text{final}} = \mathcal{F}_{\text{LLM}}(\text{concat}(\mathbf{E}_v, \mathbf{E}_{\text{word}})). \quad (7)$$

In BUS reports, clinical terms such as BI-RADS descriptors, tumor characteristics (e.g., size and location), and histopathology terms are more important than general words. Many of these terms are split into multiple sub-tokens by standard tokenizers, which increases the chance of hallucination or partial word generation. To address this, relevant clinical terms are added to the tokenizer as independent tokens before training, so the LLM embedding matrix is resized accordingly.

During the report generation stage, the vision encoder is fine-tuned starting from the multitask weights, while the language model remains frozen due to the limited dataset size. Training is optimized by combining two loss functions computed from the LLM output and the report: a cross-entropy loss over tokens and a cosine-similarity alignment loss between input and output representations.

The token-level cross-entropy loss is

$$\mathcal{L}_{\text{CE}} = - \sum_{i=1}^L \log p(x_i), \quad (8)$$

where $p(x_i)$ represents the predicted probability of token x_i at position i in a sequence of length L .

Let $\mathbf{H} \in \mathbb{R}^{L \times D}$ denote the last hidden state of the LLM and $\mathbf{Z} \in \mathbb{R}^{L \times D}$ the corresponding input embeddings (including vision tokens, prompt tokens, and report tokens). We define a cosine-similarity alignment loss as

$$\mathcal{L}_{\text{Align}} = 1 - \frac{1}{L} \sum_{i=1}^L \frac{\mathbf{H}_i \cdot \mathbf{Z}_i}{\|\mathbf{H}_i\| \|\mathbf{Z}_i\|}, \quad (9)$$

which encourages the final LLM representations to stay aligned with the image-conditioned input embeddings.

The final training objective for the report generation stage is a weighted sum of the two losses:

$$\mathcal{L} = \lambda_{\text{CE}} \mathcal{L}_{\text{CE}} + \lambda_{\text{Align}} \mathcal{L}_{\text{Align}}, \quad (10)$$

with $\lambda_{\text{CE}} = \lambda_{\text{Align}} = 0.5$ in our experiments. This joint objective helps the model match the token-level content while also maintaining a consistent alignment between visual-textual inputs and the generated report representations.

Table 1: BrEaST case distribution per descriptor category.

Descriptor	Categories	cases	Descriptor	Categories	cases
BI-RADS	2	30	Margin	Circumscribed	115
	3	37		Non-Circumscribed:	137
	4A	44		Angular	42
	4B	46		Indistinct	115
	4C	49		Microlobulated	36
Shape	5	46		Spiculated	33
	Oval	97	Echogenicity	Anechoic	15
	Round	15		Hypoechoic	148
Posterior Features	Irregular	140		Hyperechoic	9
	None	159		Isoechoic	12
	Enhancement	36		Heterogeneous	57
	Shadowing	50		Complex Cystic/Solid	11
Combined Features					
		7			

Table 2: BUS-BRA descriptor distribution

Descriptor	Categories	# of cases
BI-RADS	2	562
	3	463
	4	693
	5	157
Pathology	Benign	1268
	Malignant	607
Histology Top 10 of 28	Fibroadenoma	835
	Invasive Ductal Carcinoma	520
	Cyst	142
	Fibrocystic Changes	106
	Invasive Lobular Carcinoma	42
	Intraductal Papilloma	41
	Sclerosing Adenosis	37
	Hyperplasia	31
	Lipoma	17
	Phyllodes Tumor	13

3 Experiments

3.1 Datasets and preprocessing

We evaluate BUSTR on two publicly available breast ultrasound datasets: BrEaST [32] and BUS-BRA [33]. Both datasets provide BUS images and structured descriptors that can be used as input to the zero-shot supervisory report constructed from descriptors and radiomics.

BrEaST contains 256 BUS images with detailed BI-RADS descriptors, including BI-RADS category, lesion shape, margin (with sub-types), echogenicity, and posterior features. The dataset also includes curated lesion masks that allow radiomics feature extraction. However, the number of cases is relatively small, and some descriptor categories are highly imbalanced. For report generation, we focus on five descriptors: BI-RADS class, shape, margin (including non-circumscribed sub-types), echogenicity, and posterior features. Cases with BI-RADS category 1 (four images) are excluded from the analysis. The full descriptor distribution is summarized in Table 1.

BUS-BRA contains 1,875 BUS images with fewer descriptors but a larger number of cases. For each image, BI-RADS category, pathology (benign vs. malignant), and histology are available. All three are used in the zero-shot report generation and in the multitask training. The descriptor distribution for BUS-BRA is given in Table 2.

Table 3: Overall performance using NLG metrics. Bold indicates the best, and underlined indicates the second best.

Approaches	BLEU-1↑	BLEU-2↑	BLEU-3↑	BLEU-4↑	ROUGE-L↑	METEOR↑	CIDEr↑	
BrEaST	R2GenGPT	0.586	0.465	0.383	0.324	0.442	0.290	0.159
	R2GenCMN	0.635	0.520	0.439	0.379	0.498	0.306	0.418
	Li	0.628	0.516	0.439	0.381	0.497	0.303	0.378
	TSGET	0.633	0.523	0.445	0.386	<u>0.508</u>	0.307	0.438
	R2Gen	<u>0.639</u>	<u>0.528</u>	<u>0.450</u>	<u>0.391</u>	0.504	<u>0.310</u>	<u>0.492</u>
	Ours	0.668	0.554	0.475	0.415	0.557	0.336	0.688
BUS-BRA	R2GenGPT	0.705	0.595	0.517	0.458	0.593	0.359	<u>1.673</u>
	R2GenCMN	<u>0.722</u>	0.617	0.541	0.483	0.611	0.370	1.414
	Li	0.721	<u>0.619</u>	<u>0.543</u>	<u>0.484</u>	<u>0.617</u>	0.369	1.302
	TSGET	0.718	0.610	0.533	0.475	0.602	<u>0.371</u>	1.484
	R2Gen	0.715	0.607	0.531	0.472	0.606	0.365	1.298
	Ours	0.738	0.642	0.572	0.516	0.656	0.398	2.110

For both datasets, images are padded to obtain square slices and then resized to 224×224 pixels. To obtain robust estimates and avoid imbalanced splits, we perform five-fold cross-validation. For each fold, the training set is further split into 80% training and 20% validation. No data augmentation is applied.

3.2 Training, Inference, and Implementation Details

3.2.1 Training stages.

Training consists of two stages:

1. Multi-head vision encoder. We first train the Swin Transformer encoder with multiple descriptor heads as defined in Sec. II-C. For each dataset, the active descriptor set follows Sec. III-A (e.g., shape, margin, echogenicity, posterior features, and BI-RADS for BrEaST; BI-RADS, pathology, and histology for BUS-BRA). The encoder is trained for 100 epochs with a batch size of 8 and a learning rate of 1×10^{-4} using the multitask loss in Eq (6).
2. Report generation. In the second stage, we freeze the LLaMA language model while fine-tuning the vision encoder starting from the multitask weights obtained in Stage 1. The report generation model is trained for 25 epochs on BrEaST and 35 epochs on BUS-BRA, with a batch size of 8 and the same learning rate of 1×10^{-4} . The training objective is the combined loss in Eq. (10), based on token-level cross-entropy and a cosine-similarity alignment loss.

For both stages, the same five-fold partitions are used to prevent data leakage between training, validation, and test sets. At inference time, BUSTR receives only a BUS image as input and generates a narrative report without access to structured descriptors.

3.2.2 Implementation details.

All experiments are conducted on a single machine with an Intel Xeon Gold 6326 CPU (2.90 GHz) and NVIDIA A100 80 GB GPUs. Training all five folds requires approximately 4 hours for BrEaST and 16 hours for BUS-BRA.

3.3 Evaluation Metrics

We evaluate BUSTR with two groups of metrics: Natural Language Generation (NLG) metrics and Clinical Efficacy (CE) metrics.

3.3.1 NLG metrics.

To measure the similarity between generated reports and ground truth reports, we use BLEU-1 to BLEU-4 [34], ROUGE-L [35], METEOR [36], and CIDEr [37]. These metrics capture n-gram overlap, longest common subsequences, semantic coverage, and consensus-based similarity.

Table 4: Overall Performance using CE metrics for BrEaST dataset. Bold indicates the best, and underlined refers the second best performance.

Descriptor		R2GenGPT	R2GenCMN	Li	R2Gen	TSGET	BUSTR
BI-RADS	↑ P	0.166	0.178	0.105	<u>0.329</u>	0.218	0.356
	↑ S	0.115	0.235	0.171	<u>0.250</u>	0.206	0.258
	↑ F1	0.123	0.182	0.114	<u>0.244</u>	0.165	0.250
Shape	↑ P	0.490	0.559	0.602	0.689	0.655	<u>0.685</u>
	↑ S	0.457	0.592	0.595	<u>0.654</u>	0.638	0.706
	↑ F1	0.447	0.529	0.577	<u>0.647</u>	0.613	0.690
Echogenicity	↑ P	0.348	0.384	0.344	<u>0.415</u>	0.422	0.351
	↑ S	0.560	<u>0.568</u>	0.556	0.528	<u>0.568</u>	0.568
	↑ F1	0.428	0.445	0.424	0.453	<u>0.449</u>	0.433
Margin	↑ P	0.631	0.612	0.645	0.757	0.726	<u>0.752</u>
	↑ S	0.523	0.612	0.639	<u>0.710</u>	0.678	0.714
	↑ F1	0.496	0.559	0.629	<u>0.711</u>	0.666	0.724
Posterior Features	↑ P	0.401	<u>0.451</u>	0.401	0.556	0.427	0.402
	↑ S	0.592	0.631	<u>0.631</u>	0.635	0.572	<u>0.631</u>
	↑ F1	0.478	<u>0.517</u>	0.490	0.556	0.477	0.491

Table 5: Overall Performance using CE metrics for BUS-BRA dataset. Bold indicates the best, and underlined refers the second best performance.

Descriptor		R2GenGPT	R2GenCMN	Li	TSGET	R2Gen	BUSTR
BI-RADS	↑ P	0.472	0.511	0.333	<u>0.562</u>	0.534	0.565
	↑ S	0.468	0.516	0.428	<u>0.540</u>	0.473	0.547
	↑ F1	0.462	0.494	0.320	0.537	0.454	<u>0.534</u>
Pathology	↑ P	0.715	<u>0.819</u>	0.790	0.808	0.797	0.842
	↑ S	0.726	<u>0.797</u>	0.767	0.781	0.791	0.842
	↑ F1	0.717	<u>0.798</u>	0.766	0.786	0.793	0.838
Histology	↑ P	0.401	<u>0.472</u>	0.419	0.456	0.421	0.508
	↑ S	0.509	0.589	0.570	0.576	<u>0.576</u>	0.543
	↑ F1	0.432	<u>0.509</u>	0.477	0.498	0.484	0.510

3.3.2 CE metrics.

To assess the correctness of clinically relevant content, we compute precision (P), sensitivity (S), and F1-score (F1) for key lesion descriptors and BI-RADS category. For BrEaST, we report CE metrics for BI-RADS, shape, echogenicity, margin, and posterior features. For BUS-BRA, we evaluate BI-RADS, pathology, and histology. These metrics quantify how accurately the generated reports recover the underlying structured facts and, together with qualitative examples (e.g., Fig. 2), provide a simple form of post-hoc interpretability by verifying whether the generated text correctly recovers key lesion descriptors and BI-RADS categories.

3.4 Overall Performance

3.4.1 Natural language generation.

We compare BUSTR with five state-of-the-art (SOTA) models: R2Gen [38], R2GenCMN [39], TSGET [40], and R2GenGPT [15], originally developed for chest X-ray report generation, and Li [25], which is designed for ultrasound imaging. Table 3 summarizes the NLG performance.

BUSTR consistently outperforms all baselines on both datasets. On BrEaST, it achieves the best BLEU-4, ROUGE-L, METEOR, and CIDEr scores (0.415, 0.557, 0.336, and 0.688, respectively). On BUS-BRA, BUSTR further improves performance, reaching 0.516 BLEU-4, 0.656 ROUGE-L, 0.398 METEOR, and 2.110 CIDEr. These gains indicate that integrating a vision encoder on structured descriptors, radiomics features, and the proposed dual-level loss significantly enhances the quality and consistency of the generated BUS reports compared to existing approaches.



Ground Truth: breast ultrasound image report: the ultrasound image reveals a hypoechoic _tumor_size_ cm mass located in the center of the breast . ① the mass exhibits irregular shape and ② indistinct, angular margins, which are not circumscribed . ③ the posterior features of the mass are not visible due to its central location . ④ the echogenicity of the mass is hypoechoic, indicating a darker appearance compared to the surrounding breast issue . the presence of these features raises concerns for malignancy, and a ⑤ bi-rads category of 5 is assigned . this category indicates highly suggestive of malignancy, and further evaluation, such as biopsy, is recommended .

Domain Vocabulary

“breast” “hypoechoic” “_tumor_size_” “mass” “located” “center” “irregular” “shape” “indistinct” “angular” “margin” “not circumscribed” “posterior” “features” “not visible” “echogenicity” “malignancy” “bi-rads” “category” “5”

Li: breast ultrasound image report the tumor is located in the center of the breast measuring _tumor_size_ cm in diameter . ③ the posterior features of the tumor exhibit shadowing . ① the shape of the tumor is irregular . ④ the echogenicity of the tumor is hypoechoic . the tumor is hypoechoic . ② the margin of the tumor is not circumscribed with an irregular shape and indistinct margin raise concerns about its nature . the lack of posterior features and hypoechoic echogenicity further contribute to the lesion . the lesion . ⑤ bi-rads category 4c .

R2Gen: breast ultrasound image report the ultrasound image reveals a hypoechoic _tumor_size_ cm mass located in the center of the breast with an ① irregular shape and ② indistinct margins . ③ the tumors posterior features are not visible due to its central location . ④ the echogenicity of the tumor is hypoechoic indicating a darker appearance compared to the surrounding breast tissue . ⑤ bi-rads category 4c the presence of irregular shape indistinct margins and hypoechoic echogenicity raises moderate suspicion for malignancy . further evaluation such as biopsy is recommended to determine the nature of the lesion .

BUSTR: breast ultrasound image report: the tumor is located in the center of the breast , measuring 1.0 cm in diameter . ③ the posterior features of the tumor are not visible . ① the shape of the tumor is irregular . ② the margin of the tumor is not circumscribed . ④ the echogenicity of the tumor is hypoechoic . the echogenicity of the tumor is hypoechoic . the tumor s irregular shape and indistinct margin are highly suggestive of malignancy . ⑤ bi-rads category : 5 .

TSGET: breast ultrasound image report the ultrasound image reveals a hypoechoic mass located centrally in the breast measuring _tumor_size_ cm in diameter . ③ the posterior features of the tumor exhibit shadowing . ① the shape of the tumor is irregular . ② the margin of the tumor is not circumscribed appearing indistinct . ④ the echogenicity of the tumor is hypoechoic . the tumor is hypoechoic . the presence of an irregular shape indistinct margin and angular margins and hypoechoic echogenicity of the tumor further supports this finding warrants a high suspicion for malignancy . ⑤ bi-rads category 4c is assigned indicating a high suspicion for malignancy that cannot be confidently characterized as benign or malignant based on imaging features alone .

Figure 2: Qualitative comparison between top-performing models. Different colors are used to show each predicted descriptor. Highlighted texts are incorrect predictions.

3.4.2 Clinical efficacy.

Tables 4 and 5 report CE metrics for descriptor prediction. For BrEaST, BUSTR achieves the highest precision, sensitivity, and F1-score for the BI-RADS category, and the best F1-score for margin classification ($F1 = 0.724$), while also providing the strongest overall balance across shape, echogenicity, and posterior features. Some baselines, such as R2Gen and TSGET, obtain slightly higher precision or F1-scores on individual descriptors (e.g., echogenicity or posterior features), but their improvements are localized and do not extend across all metrics.

For BUS-BRA, BUSTR consistently outperforms all baselines in precision for BI-RADS, pathology, and histology, and achieves the highest F1-scores for pathology and histology. For BI-RADS, BUSTR attains the best precision and a near-best F1-score that is comparable to TSGET. Overall, these results indicate that BUSTR improves both textual quality and clinical faithfulness of the generated reports, especially for clinically critical targets such as BI-RADS and pathology.

3.5 Statistical Analysis

To assess whether BUSTR’s performance gains are robust across folds, we perform paired two-sided t -tests on the five-fold test scores for the automatic text metrics (BLEU-4, ROUGE-L, METEOR, and CIDEr). For each dataset, BUSTR is compared with the strongest CIDEr baseline (R2Gen for BrEaST and R2GenGPT for BUS-BRA). On BrEaST, BUSTR improves ROUGE-L, METEOR, and CIDEr over R2Gen with statistically significant differences ($p < 0.05$), while the gain in BLEU-4 is positive but not significant ($p \approx 0.14$). On BUS-BRA, BUSTR achieves statistically significant improvements over R2GenGPT for all four metrics ($p < 0.01$ in each case). These tests indicate that the improvements reported in Table 3 are consistent across folds rather than due to random variation.

Table 6: The performance of each contribution of the model and other different approaches using NLG metrics. Bold indicates the best, and underlined indicates the second best.

	Approaches	BLEU-1↑	BLEU-2↑	BLEU-3↑	BLEU-4↑	ROUGE-L↑	METEOR↑	CIDEr↑
BrEaST	Base Model	0.634	0.521	0.444	0.387	0.487	0.330	0.537
	Vision Only	0.659	0.545	0.465	0.405	0.548	0.331	0.566
	Loss Only	0.658	0.542	0.459	0.398	0.541	0.328	0.553
	CE + Cos	0.669	0.556	0.476	0.416	<u>0.556</u>	0.337	<u>0.664</u>
	CE * Cos	0.663	0.549	0.467	0.407	0.551	0.332	0.552
	mean(CE, Cos)	<u>0.668</u>	<u>0.554</u>	<u>0.475</u>	<u>0.415</u>	0.557	<u>0.336</u>	0.688
BUS-BRA	Base Model	0.717	0.615	0.540	0.483	0.608	0.392	1.924
	Vision Only	0.724	0.623	0.549	0.494	0.619	0.398	1.920
	Loss Only	0.728	0.628	0.555	0.498	0.643	0.392	2.087
	CE + Cos	<u>0.736</u>	<u>0.639</u>	0.568	0.512	0.655	0.398	2.155
	CE * Cos	0.728	0.631	0.561	0.505	0.649	0.392	1.974
	mean(CE, Cos)	0.738	0.642	0.572	<u>0.516</u>	<u>0.656</u>	0.398	<u>2.110</u>
	max(CE, Cos)	0.730	0.638	<u>0.570</u>	0.517	0.657	<u>0.394</u>	1.952

3.6 Ablation Study

To quantify the contribution of each component, we conduct ablation experiments summarized in Table 6. We consider the following variants:

- Base Model: a basic vision encoder (pre-trained Swin Transformer) with a single linear projection to the word embedding space and standard cross-entropy loss.
- Vision Only: the base model where the vision encoder is replaced by our descriptor-aware multi-head encoder, while the loss function remains standard cross-entropy.
- Loss Only: the base vision encoder with the combined objective based on token-level cross-entropy and cosine-similarity alignment loss between the LLM’s final hidden states and the input embeddings.
- Full BUSTR: our complete model using both the descriptor-aware multi-head vision encoder and the dual-level loss. We further evaluate different choices for the combination function \mathcal{F} (sum, product, mean, max) over L_{CE} and L_{Align} .

The results show that both the vision encoder and the loss design contribute meaningfully to performance. On BrEaST, replacing the base encoder with our multi-head encoder (Vision Only) improves BLEU-4 from 0.387 to 0.405, while using only the combined loss (Loss Only) yields BLEU-4 of 0.398. When both contributions are combined, BUSTR achieves BLEU-4 of 0.415 and the highest CIDEr score (0.688). Similar trends are observed on BUS-BRA, where the full model reaches 0.516 BLEU-4 and 2.110 CIDEr.

Across combination functions, taking the mean of L_{CE} and L_{Align} provides a good balance between token-level accuracy and global consistency of the hidden representations, and is adopted as the default choice for BUSTR.

4 Discussion

Our results suggest that supervisory reports derived from structured descriptors are a viable supervision signal when human-written paired reports are not available. BUSTR outperforms all baselines in BLEU-4, ROUGE-L, METEOR, and CIDEr on both datasets (Table 3). Paired two-sided t -tests on the five-fold test scores indicate that, on BrEaST, the gains in ROUGE-L, METEOR, and CIDEr over R2Gen are statistically significant ($p < 0.05$), whereas the improvement in BLEU-4 is smaller and not significant ($p \approx 0.14$). On BUS-BRA, BUSTR achieves statistically significant improvements over R2GenGPT for all four metrics ($p < 0.01$). A likely reason is that these supervisory reports provide a clean and consistent training signal: they are deterministically constructed from structured descriptors and radiomics and avoid some of the stylistic variability and omissions present in narrative reports. The multi-head vision encoder and multitask loss further contribute to these gains. By predicting multiple lesion descriptors through separate heads and optimizing their joint loss, the encoder learns descriptor-aware visual features. The ablation study

(Table 6) shows that replacing the base encoder with the multi-head encoder (Vision Only) improves BLEU-4 and CIDEr, suggesting that explicit descriptor supervision produces visual representations that are better aligned with the structured information used to build the reports.

The dual-level objective function also improves alignment between generated reports and ground truth reports. The Loss Only variant, which uses the combined token-level cross-entropy and cosine-similarity alignment loss with a base encoder, already improves NLG metrics over the base model, and the full BUSTR (multi-head encoder plus dual loss) achieves the best performance on all NLG metrics across both datasets (Table 6). Taking the mean of \mathcal{L}_{CE} and \mathcal{L}_{Align} offers a good balance between local token accuracy and global consistency of the hidden representations. Cross-entropy encourages correct next-token prediction given the image-conditioned context, while the alignment term encourages the final LLM hidden states to remain close to the input embedding trajectory formed by visual tokens, prompts, and ground truth reports. Empirically, this leads to outputs that are both fluent and better grounded in the underlying structured facts.

From a clinical perspective, the CE results highlight both strengths and remaining challenges. On BrEaST, BUSTR achieves the highest precision, sensitivity, and F1-score for BI-RADS category and the best F1-score for margin, while maintaining strong performance on shape (Table 4). On BUS-BRA, it attains the best precision for BI-RADS, pathology, and histology, and the best F1-scores for pathology and histology, with BI-RADS F1 comparable to the best baseline (Table 5). These patterns suggest that BUSTR is particularly effective for clinically critical targets such as BI-RADS and pathology, which are directly and strongly supervised both in the multi-head encoder and in the reports. Qualitative examples in Fig. 2 show that BUSTR produces more coherent sentences and more structured tumor descriptions, with fewer misclassifications of critical information than the baselines. Tumor size estimation remains more difficult, likely because it is a continuous quantity that is sensitive to noise and scaling; we therefore use a dedicated regression head at inference time and insert the predicted size into the report text instead of relying on the language model to infer it.

Despite these promising results, our study has two main limitations. First, the evaluation is based on two specific BUS datasets, BrEaST and BUS-BRA, which have limited sample sizes and incomplete annotations. BrEaST is relatively small and imbalanced, and neither dataset provides real narrative radiology reports; instead, we rely on structured descriptors and, when available, lesion masks to construct reports. As a result, reporting style diversity and coverage of rare findings are constrained by the available labels, and the performance and generalizability of BUSTR on larger, more heterogeneous datasets remain to be established. Second, our assessment is entirely algorithmic: we use automatic NLG and CE metrics, but we do not yet include radiologists in the loop. There are no reader studies to evaluate clinical usefulness, trust, or impact on workflow, or to measure whether BUSTR’s narrative outputs improve interpretability compared to conventional quantitative predictions (e.g., BI-RADS scores alone). Incorporating expert feedback and prospective radiologist-in-the-loop evaluation will be essential to understand how the proposed system behaves in real clinical practice, how its narrative reports are perceived by end-users, and how it might be integrated into existing reporting pipelines.

5 Conclusion

We presented BUSTR, a framework for breast ultrasound (BUS) report generation that does not require paired image-report data. BUSTR constructs reports from descriptors and radiomics features, learns descriptor-aware visual representations with a multi-head Swin encoder trained under a multitask loss, and aligns vision and language using a dual-level objective that combines token-level cross-entropy with a cosine-similarity alignment term. Experiments on the BrEaST and BUS-BRA datasets show that BUSTR outperforms recent baselines on standard NLG metrics and improves clinical efficacy for key targets such as BI-RADS category and pathology, indicating that descriptor- and radiomics-based supervision can provide a viable training signal when narrative reports are unavailable.

In addition to improving prediction performance, BUSTR generates narrative reports that explicitly connect lesion descriptors and radiomics-derived attributes to the final assessment, offering a potential path toward more interpretable BUS AI systems. Future work will evaluate the framework on larger, more diverse datasets and include radiologist-in-the-loop studies to assess clinical usefulness, trust, and perceived interpretability in real-world workflows.

References

- [1] Thomas M Kolb, Jacob Lichy, and Jeffrey H Newhouse. Comparison of the performance of screening mammography, physical examination, and breast us and evaluation of factors that influence them: an analysis of 27,825 patient evaluations. *Radiology*, 225(1):165–175, 2002.
- [2] IHS Markit. The complexities of physician supply and demand: Projections from 2015 to 2030. Technical report, 2017.

- [3] Dengdi Sun, Changxu Dong, Yuchen Yan, Bo Jiang, Yayang Duan, Zhengzheng Tu, and Chaoxue Zhang. Challenge-aware u-net for breast lesion segmentation in ultrasound images. *Pattern Recognition*, page 111851, 2025.
- [4] Bryar Shareef, Aleksandar Vakanski, Phoebe E. Freer, and Min Xian. Estan: Enhanced small tumor-aware network for breast ultrasound image segmentation. *Healthcare*, 10(11):2262, 2022.
- [5] TR Mahesh, Surbhi Bhatia Khan, Kritika Kumari Mishra, Saeed Alzahrani, and Mohammed Alojail. Enhancing diagnostic precision in breast cancer classification through efficientnetb7 using advanced image augmentation and interpretation techniques. *International Journal of Imaging Systems and Technology*, 35(1):e70000, 2025.
- [6] Y. Zhang, M. Xian, H.D. Cheng, B. Shareef, J. Ding, F. Xu, K. Huang, B. Zhang, C. Ning, and Y. Wang. Busis: A benchmark for breast ultrasound image segmentation. *Healthcare (Basel)*, 10(4):729, 2022.
- [7] Ruili Li, Ruiyu Li, Eichi Takaya, Zizhen Lin, Tomoya Kobayashi, Nanako Matsuda, and Takuya Ueda. Bcs-net: Multi-task breast cancer screening network enhanced by multi-modality attention. In *ICASSP 2025 - 2025 IEEE International Conference on Acoustics, Speech and Signal Processing (ICASSP)*, pages 1–5, 2025.
- [8] Haoyuan Chen, Yonghao Li, Jiadong Zhang, Long Yang, Yiqun Sun, Yaling Chen, Shichong Zhou, Zhenhui Li, Xuejun Qian, Qi Xu, and Dinggang Shen. An alignment and imputation network (ainet) for breast cancer diagnosis with multimodal multi-view ultrasound images. *IEEE Transactions on Medical Imaging*, pages 1–1, 2025.
- [9] Bryar Shareef, Min Xian, Aleksandar Vakanski, and Haotian Wang. Breast ultrasound tumor classification using a hybrid multitask cnn-transformer network. In *Medical Image Computing and Computer-Assisted Intervention (MICCAI)*, 2023.
- [10] Tatiana Tommasi, Francesco Orabona, and Barbara Caputo. An svm confidence-based approach to medical image annotation. In *Workshop of the Cross-Language Evaluation Forum for European Languages*, pages 696–703. Springer, 2008.
- [11] Julien Gobet, Patrick Ruch, and Xin Zhou. Query and document expansion with medical subject headings terms at medical imageclef 2008. In *Evaluating Systems for Multilingual and Multimodal Information Access: 9th Workshop of the Cross-Language Evaluation Forum, CLEF 2008, Aarhus, Denmark, September 17-19, 2008, Revised Selected Papers 9*, pages 736–743. Springer, 2009.
- [12] Mehreen Sirshar, Muhammad Faheem Khalil Paracha, Muhammad Usman Akram, Norah Saleh Alghamdi, Syeda Zainab Yousuf Zaidi, and Tatheer Fatima. Attention based automated radiology report generation using cnn and lstm. *Plos one*, 17(1):e0262209, 2022.
- [13] Xinyi Wang, Grazziela Figueiredo, Ruizhe Li, Wei Emma Zhang, Weitong Chen, and Xin Chen. A survey of deep learning-based radiology report generation using multimodal data. *arXiv preprint arXiv:2405.12833*, 2025.
- [14] Zhanyu Wang, Lingqiao Liu, Lei Wang, and Luping Zhou. METransformer: Radiology report generation by transformer with multiple learnable expert tokens. In *Proceedings of the IEEE/CVF Conference on Computer Vision and Pattern Recognition (CVPR)*, pages 16302–16312, 2023.
- [15] Wang, Z. and Liu, L. and Wang, L. and Zhou, L. R2gengpt: Radiology report generation with frozen llms. *Meta-Radiology*, 1(3):100033, 2023.
- [16] Zhaoyi Sun, Hanley Ong, Patrick Kennedy, Liyan Tang, Shirley Chen, Jonathan Elias, Eugene Lucas, George Shih, and Yifan Peng. Evaluating gpt-4 on impressions generation in radiology reports. *Radiology*, 307(5):e231259, 2023.
- [17] Ankit Pal and Malaikannan Sankarasubbu. Gemini goes to med school: exploring the capabilities of multimodal large language models on medical challenge problems & hallucinations. In *Proceedings of the 6th Clinical Natural Language Processing Workshop*, pages 21–46, 2024.
- [18] Vignav Ramesh, Nathan A Chi, and Pranav Rajpurkar. Improving radiology report generation systems by removing hallucinated references to non-existent priors. In *Machine Learning for Health*, pages 456–473. PMLR, 2022.
- [19] Difei Gu, Yunhe Gao, Yang Zhou, Mu Zhou, and Dimitris Metaxas. RadAlign: Advancing radiology report generation with vision-language concept alignment. *arXiv preprint arXiv:2501.07525*, 2025.
- [20] Daniel Parres, Alberto Albiol, and Roberto Paredes. Improving radiology report generation quality and diversity through reinforcement learning and text augmentation. *Bioengineering*, 11(4):351, 2024.
- [21] Raja Mallina and Bryar Shareef. Xbusnet: Text-guided breast ultrasound segmentation via multimodal vision-language learning. *Diagnostics*, 15(22):2849, 2025.

- [22] Boyu Zhang, Aleksandar Vakanski, and Min Xian. Bi-rads-net-v2: a composite multi-task neural network for computer-aided diagnosis of breast cancer in ultrasound images with semantic and quantitative explanations. *IEEE Access*, 11:79480–79494, 2023.
- [23] Laurie R. Margolies, Gaurav Pandey, Eliot R. Horowitz, and David S. Mendelson. Breast imaging in the era of big data: Structured reporting and data mining. *AJR American Journal of Roentgenology*, 206(2):259–264, 2016.
- [24] Shuang Ge, Qiongyu Ye, Wenquan Xie, Desheng Sun, Huabin Zhang, Xiaobo Zhou, and Kehong Yuan. Ai-assisted method for efficiently generating breast ultrasound screening reports. *Current Medical Imaging*, 19(2):149–157, 2023.
- [25] Jun Li, Tongkun Su, Baoliang Zhao, Faqin Lv, Qiong Wang, Nassir Navab, Ying Hu, and Zhongliang Jiang. Ultrasound report generation with cross-modality feature alignment via unsupervised guidance. *IEEE Transactions on Medical Imaging*, 2024.
- [26] Chung-Ming Lo and Hui-Ru Chen. Automated breast imaging report generation based on the integration of multiple image features in a metadata format for shared decision-making. *Health informatics journal*, 30(3):14604582241288460, 2024.
- [27] Haojun Qin, Lei Zhang, and Quan Guo. Computer-aided diagnosis system for breast ultrasound reports generation and classification method based on deep learning. *Applied Sciences*, 13(11):6577, 2023.
- [28] Khadija Azhar, Byoung-Dai Lee, Shi Sub Byon, Kyu Ran Cho, and Sung Eun Song. Ai-powered synthesis of structured multimodal breast ultrasound reports integrating radiologist annotations and deep learning analysis. *Bioengineering*, 11(9):890, 2024.
- [29] Jaeyoung Huh, Hyun Jeong Park, and Jong Chul Ye. Breast ultrasound report generation using LangChain. *arXiv preprint arXiv:2312.03013*, 2023.
- [30] Hugo Touvron, Louis Martin, Kevin Stone, Peter Albert, Amjad Almahairi, Yasmine Babaei, Nikolay Bashlykov, Soumya Batra, Prajjwal Bhargava, Shruti Bhosale, et al. Llama 2: Open foundation and fine-tuned chat models. *arXiv preprint arXiv:2307.09288*, 2023.
- [31] Ze Liu, Yutong Lin, Yue Cao, Han Hu, Yixuan Wei, Zheng Zhang, Stephen Lin, and Baining Guo. Swin transformer: Hierarchical vision transformer using shifted windows. In *Proceedings of the IEEE/CVF international conference on computer vision*, pages 10012–10022, 2021.
- [32] Anna Pawłowska, Anna Ćwierz-Pieńkowska, Agnieszka Domalik, Dominika Jaguś, Piotr Kasprzak, Rafał Matkowski, Łukasz Fura, Andrzej Nowicki, and Norbert Żołek. Curated benchmark dataset for ultrasound based breast lesion analysis. *Scientific Data*, 11(1):148, 2024.
- [33] Wilfrido Gómez-Flores, Maria Julia Gregorio-Calas, and Wagner Coelho de Albuquerque Pereira. Bus-bra: a breast ultrasound dataset for assessing computer-aided diagnosis systems. *Medical Physics*, 51(4):3110–3123, 2024.
- [34] Kishore Papineni, Salim Roukos, Todd Ward, and Wei-Jing Zhu. Bleu: a method for automatic evaluation of machine translation. In *Proceedings of the 40th annual meeting of the Association for Computational Linguistics*, pages 311–318, 2002.
- [35] Chin-Yew Lin. Rouge: A package for automatic evaluation of summaries. In *Text summarization branches out*, pages 74–81, 2004.
- [36] Satanjeev Banerjee and Alon Lavie. Meteor: An automatic metric for mt evaluation with improved correlation with human judgments. In *Proceedings of the acl workshop on intrinsic and extrinsic evaluation measures for machine translation and/or summarization*, pages 65–72, 2005.
- [37] Ramakrishna Vedantam, C Lawrence Zitnick, and Devi Parikh. Cider: Consensus-based image description evaluation. In *Proceedings of the IEEE conference on computer vision and pattern recognition*, pages 4566–4575, 2015.
- [38] Zhihong Chen, Yan Song, Tsung-Hui Chang, and Xiang Wan. Generating radiology reports via memory-driven transformer. In *Proceedings of the 2020 Conference on Empirical Methods in Natural Language Processing (EMNLP)*, pages 1439–1449, 2020.
- [39] Zhihong Chen, Yaling Shen, Yan Song, and Xiang Wan. Cross-modal memory networks for radiology report generation. In *Proceedings of the 59th Annual Meeting of the Association for Computational Linguistics and the 11th International Joint Conference on Natural Language Processing (Volume 1: Long Papers)*, pages 5904–5914, 2021.
- [40] Xiulong Yi, You Fu, Ruiqing Liu, Hao Zhang, and Rong Hua. Tsget: Two-stage global enhanced transformer for automatic radiology report generation. *IEEE Journal of Biomedical and Health Informatics*, 28(4):2152–2162, 2024.